TRANSITIONAL SHOCK-WAVE BOUNDARY LAYER INTERACTION OVER A COMPRESSION RAMP

Nikhil Mahalingesh, Sébastien Piponniau, Pierre Dupont

12th International Symposium on Turbulence and Shear Flow Phenomena (TSFP12)
Osaka, Japan (Online), July 19-22, 2022

TRANSITIONAL SHOCK-WAVE BOUNDARY LAYER INTERACTION OVER A COMPRESSION RAMP

Nikhil Mahalingesh
Aix Marseille Univ, CNRS, IUSTI
Marseille, France
nikhil.mahalingesh@univ-amu.fr

Sébastien Piponniau
Aix Marseille Univ, CNRS, IUSTI
Marseille, France
sebastien.piponniau@univ-amu.fr

Pierre Dupont
Aix Marseille Univ, CNRS, IUSTI
Marseille, France
pierre.dupont@univ-amu.fr

ABSTRACT

Experiments are performed to study the interaction between shock-waves and a laminar boundary layer on a compression ramp at Mach 1.66. Pitot probe measurements and hot-wire anemometry are complemented with Schlieren visualisation, while Reynolds number is varied by a factor of two. The results suggest a "fully laminar" type of interaction where transition of the boundary layer occurs downstream of reattachment. On the contrary, oblique shock-wave laminar boundary layer interactions resulted in a "transitional" type of interaction with transition occurring at reattachment, for similar freestream conditions and equivalent shock strength. This difference in the type of interaction resulted in subtle deviations in the relative length and time scales of the shock-wave boundary layer interaction. The non-dimensional lengths of interactions, based on mass balance across the interaction, were similar for the two geometrical configurations, but the evolution of these length scales with increasing Reynolds number were found to be different. The Strouhal number associated with low frequency unsteadiness matched across both the configurations, with typical time scales associated with transitional mechanisms in oblique shock reflection, "delayed" in the compression ramp measurements.

INTRODUCTION

The interaction between shock-waves and boundary layers (SBLI) is a classical flow phenomenon in the field of aerodynamics. It is found in a number of real-world applications such as transonic aerofoils, rocket nozzles, supersonic inlets, high-speed engines, etc. and is usually characterised by a number of unfavourable effects including separation of the boundary layer, intense thermal loading, structural fatigue, leading to unsteadiness of the associated shock-waves. Consequently, SBLIs have been a subject of research since the 1940s (Ackeret *et al.*, 1947). Experiments and numerical simulations have been performed for various geometrical configurations (such as oblique shock impingement, compression ramps, aerofoils, compressor and/or turbine blades, etc.) and for various flow parameters, including different Mach and Reynolds numbers. These studies have shed light on the spatial scales (Dupont *et al.*, 2006; Souverein *et al.*, 2013) and characteristic frequencies (Erengil & Dolling, 1991; Piponniau *et al.*, 2009; Touber & Sandham, 2009) of the flow. Délery *et al.* (1986) reviewed some of the early studies on the topic, while Dolling (2001) provided some perspectives for future research. Clemens & Narayanaswamy (2014) recently provided a detailed retrospection of the prevailing debate on the origins of the low frequency unsteadiness. Comprehensive reviews on the subject include books by Smits & Dussauge (2006), Doerffer *et al.* (2010) and Babinsky & Harvey (2011).

However, limitations from an experimental and computational point of view had restricted much of the focus on turbulent interactions. And hence, attention to the interaction between shock-waves and laminar boundary layers had been relatively lower. Recent advancements in experimental techniques and computational resources, together with emerging focus on sustainability and increased efficiency (Commission *et al.*, 2011), have renewed interest on laminar interactions. As part of the European TFAST project, experiments were performed to study such interactions at the IUSTI laboratory of Aix-Marseille University, involving an oblique shock-wave impinging on a laminar boundary layer. The results showed a relatively long length of interaction with large aspect ratios compared to turbulent interactions (Diop *et al.*, 2017). Further, temporal measurements revealed several frequencies being amplified along the interaction, with the low frequency unsteadiness of the separation region being much higher than that of turbulent interactions (Diop *et al.*, 2016). Several open questions were left unanswered, including the specific effects of transitional mechanisms on the spatial and temporal scales of the interaction (Diop *et al.*, 2019).

The current work is an extension of those experiments, being performed with a compression ramp geometry as opposed to an oblique shock reflection case. The paper discusses the interaction between a laminar boundary layer and a 6° compression ramp at Mach 1.66. Reynolds number is varied by a factor of two to investigate its effect on the interaction. The experimental setup and methodology are detailed in the following section, describing the Pitot probe, hot-wire anemometry and Schlieren imaging. The initial part of the results focuses on the validation of the laminar boundary layer and canonical nature of the ramp SBLI. The latter part highlights the differences in length and time scales between the

compression ramp and oblique SBLI. These differences are addressed in the discussion section and conclusions are drawn.

EXPERIMENTAL METHODOLOGY

The experiments are conducted in the supersonic wind tunnel of IUSTI laboratory of Aix-Marseille University. It is a closed-loop hypo-turbulent facility which can be continuously operated up to four hours without significant changes in freestream properties. The freestream Mach number is 1.66 for a test-section of 170 mm in spanwise width and a height of 105 mm. The compression ramp consists of an initial flat section with a sharp leading edge and a 6° deflection at 115 mm from the leading edge. This geometry is placed at a height of 25 mm from the floor of the wind tunnel as shown in Figure 1.

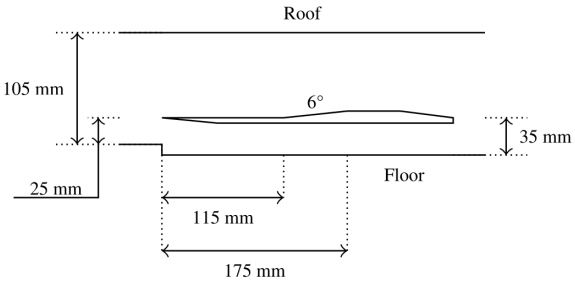

(a) Schematic of Geometry.

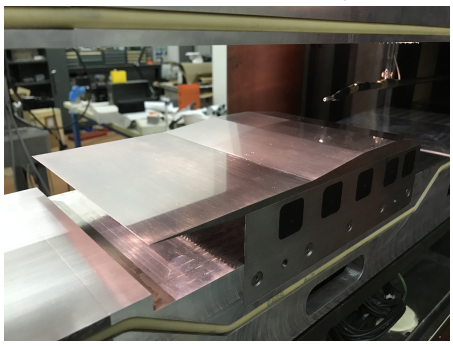

(b) Picture of Geometry.

Figure 1: Compression Ramp.

Experiments are repeated for different freestream total pressures, corresponding to different unit Reynolds numbers. Table 1 describes the equivalent unit Reynolds number (Re_u) and the Reynolds number based on the location of the corner (Re_c) for different freestream total pressures (P_0).

Table 1: Operating conditions of the experiments.

P_0 [atm]	Re_u $\left[m^{-1}\right]$ $\left(\times 10^6\right)$	Re_c $\left(\times 10^6\right)$
0.4	5.61	0.65
0.6	8.37	0.96
0.8	11.01	1.27

Pitot probe and hot-wire measurements are made in the vertical plane containing the streamwise and wall-normal directions, at the mid-span of the wind tunnel. The supersonic Pitot probe has a flat tip of 0.15 mm in height and is used for measurements of the laminar boundary layer profile, with a spatial resolution of 0.05 mm in the wall-normal direction. Longitudinal explorations are also made with the Pitot probe outside the boundary layer at a height of 5 mm from the wall with a spatial resolution of 1 mm in the streamwise direction.

External measurements of mass-flux fluctuations are also made using hot-wire anemometry with a tungsten and platinum wire of 2.5 μm diameter. The Streamline amplifier by Dantec Dynamics is used in symmetrical bridge configuration, operating in constant temperature mode with an overheat ratio of 0.8. The effective frequency bandwidth of the anemometer is approximately 150 kHz (depending on the unit Reynolds number). The calibration of the anemometer is not performed and hence the resulting spectral data are analysed in arbitrary units of the measured voltage. Temporal acquisition is obtained using National Instruments system (NI6133) at a sampling frequency of 400 kHz for 10 seconds, resulting in four million points of acquisition.

Flow visualisation is carried out with a conical Schlieren setup with a low-speed acquisition system. A classical full-frame digital SLR camera (Nikon D700) is used, having a CMOS sensor with a pixel size of 8.45 μm and a maximum resolution of 4256 $\times$ 2832 pixels with a exposure time of 150 μs.

RESULTS

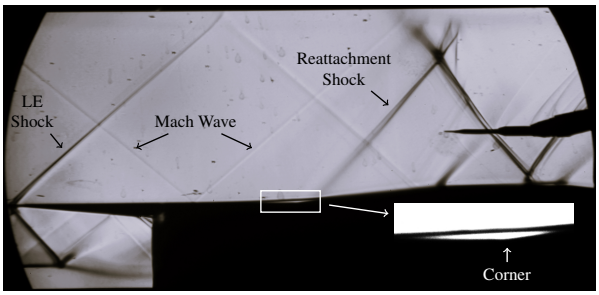

Figure 2: Schlieren visualisation at $Re_c = 0.65 \times 10^6$.

Figure 2 shows the Schlieren image for the lowest Reynolds number. A weak shock-wave from the leading edge of the ramp (annotated by LE Shock) can be seen. A weak Mach wave is seen originating from the roof of the wind tunnel upstream of the leading edge. This Mach wave is due to a microscopic structural discontinuity between the end of the diverging section of the nozzle and the start of the test section. Looking closely near the corner, it can be seen that the boundary layer separates a few millimetres upstream of the corner and consequently re-attaches downstream of the corner. A separation bubble is visible between the points of separation and reattachment (identified by the small bright white region). Separation of the boundary layer is not characterised by a distinct shock-wave, but rather weak compression waves which cannot be seen by Schlieren imaging. However diffuse compression waves are observed at reattachment, which coalesce further away from the wall and merge in to a shock-wave.

Measurements of the laminar boundary layer are made over a simple flat plate using the Pitot probe. The geometry

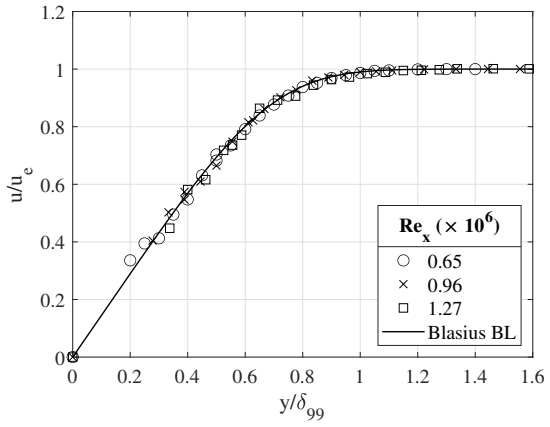

Figure 3: Boundary layer velocity profiles for various streamwise locations and comparison with Blasius profile.

and setup of the flat plate is identical to the compression ramp, and is used mainly to study the supersonic laminar boundary layer. As the geometry is placed at a height from the floor of the wind tunnel, a new natural laminar boundary layer develops from the leading edge. These measurements are repeated for the same three Reynolds numbers of the compression ramp and are shown in similarity coordinates (Figure 3). The boundary layer has a distinct linear section and having a thickness of less than 1 mm. The measurements collapse on top of each other and agree well with the Blasius boundary layer profile (the compressible Blasius boundary layer equations are solved numerically to obtain the theoretical results). These measurements confirm the laminar nature of the boundary layer for the three Reynolds numbers for the flat plate. The nature of the boundary layer is expected to be same over the compression ramp given the similarity of two geometrical setups.

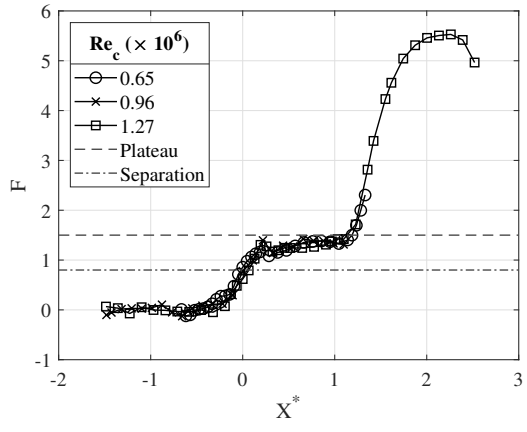

Figure 4: Free interaction theory.

Longitudinal measurements using the Pitot probe in the external flow are plotted in terms of the free-interaction coefficient (Chapman *et al.*, 1958) in Figure 4. The coefficient of free-interaction ($F(X^*)$) is determined according to Equation 1, which takes into account the change in Reynolds number through the skin-friction coefficient.

$$\frac{p-p_0}{q_0} = F(X^*)\sqrt{\frac{2c_f}{\left(M^2-1\right)^{(1/2)}}} \tag{1}$$

Standard values of the coefficient of free-interaction from various studies of laminar SBLIs (Babinsky & Harvey, 2011) at separation and plateau are also plotted in Figure 4. The streamwise coordinates are normalised with respect to the location of the corner ($X^* = 1$) and the mean location of boundary layer separation ($X^* = 0$). The mean location of separation is determined by identifying the inflection point in the gradient of pressure measurements. The measurements show a classical two-step pressure rise characteristic of separated SBLIs for the three Reynolds numbers. The values predicted by free-interaction theory at separation and over the plateau region are well reproduced by the experiments, validating the canonical nature of the measurements.

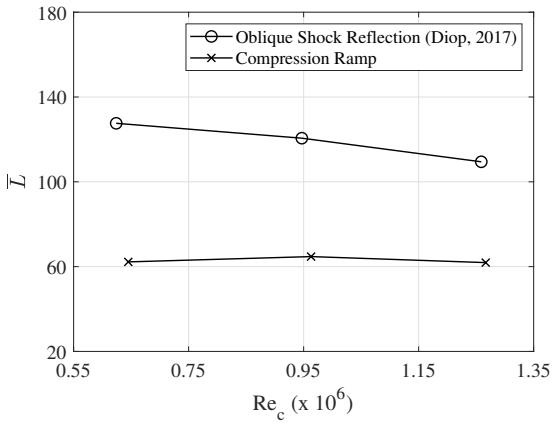

Figure 5: Variation of non-dimensional length of interaction for the three Reynolds numbers.

Additionally, Pitot measurements provide quantitative insight into the upstream influence of the SBLI through the length of interaction, which is defined as the streamwise distance between the compression corner and the mean location of boundary layer separation. Figure 5 shows the evolution of this non-dimensional length of interaction ($\bar{L}$) (normalised with the compressible displacement thickness of the boundary layer at the point of separation) for the three Reynolds numbers. It seems that the non-dimensional length of interaction is nearly constant for the three Reynolds numbers. Furthermore, Figure 5 compares the lengths of interaction to the oblique shock reflection of Diop (2017) for a flow deflection of 3°. The inviscid location of the impingement shock-wave is used as the length scale for the Reynolds number for the oblique SBLI results. The lengths of interaction in the compression ramp cases are lower by 47% on average, compared to the oblique shock reflection cases.

Souverein *et al.* (2013) proposed a scaling model for the length scales of shock-wave boundary layer interactions taking into account the effect of different geometrical configurations. This non-dimensional length scale is defined according to Equation 2, where δ^* is the compressible displacement thickness at separation, β is the inviscid shock-wave angle and φ is the imposed flow deflection.

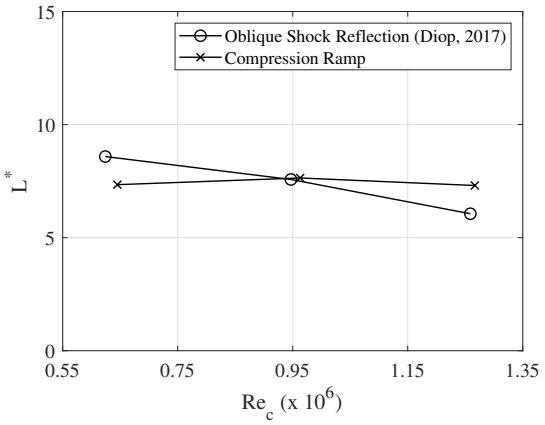

Figure 6: Scaling of length of interaction using Souverein *et al.* (2013) model.

$$L^* = \bar{L}\left(\frac{\sin(\beta)\sin(\varphi)}{\sin(\beta-\varphi)}\right) = \frac{L}{\delta^*}\left(\frac{\sin(\beta)\sin(\varphi)}{\sin(\beta-\varphi)}\right) \qquad (2)$$

The variation of this length scale (L^*) for the three Reynolds numbers is shown in Figure 6. It can be seen that the scaling significantly reduces the difference in lengths between the two geometrical configurations, with the mean difference being 12%.

Additionally, it is of interest to note that while the length scales are nearly constant for the compression ramp configuration, the same cannot be said for the oblique SBLI. Figures 5 and 6 show that the length of interaction is decreasing with increasing Reynolds numbers. This difference is addressed in the discussion section, after presenting the temporal results.

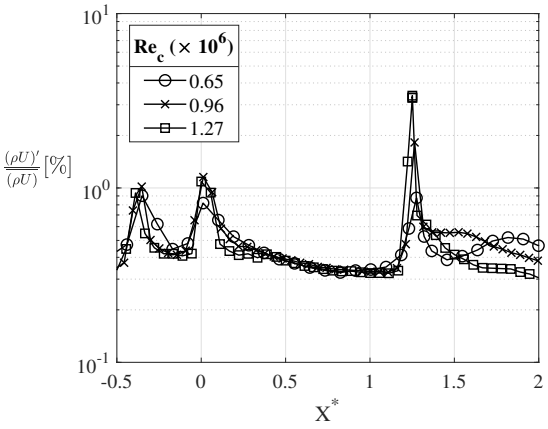

Figure 7: Longitudinal evolution of non-dimensional root-mean square of mass-flux for the three Reynolds numbers.

Moving to the time scales of the SBLI, hot-wire anemometry gives insight into the temporal aspects of the flow. External longitudinal measurements are made over the interaction at 23 mm from the wall. This height is chosen such that the interaction of the probe with the SBLI is minimal, verified by Schlieren imaging. Generally, the hot-wire anemometer is sensitive to fluctuations of total temperature, mass-flux and Mach number of the flow. In the potential region of the flow (23 mm from the wall), where the Mach number is greater than 1.4 and for a high overheat of 0.8, voltage fluctuations of the anemometer can be directly related to mass-flux fluctuations through the King's law coefficient (Morkovin, 1956; Dupont, 1990). The longitudinal evolution of the non-dimensional root-mean square (RMS) of these fluctuations are shown in Figure 7 for the three Reynolds numbers. The streamwise coordinates are normalised similar to Figure 4.

The first point measured upstream of the interaction is an indication of the freestream noise of the wind tunnel and is around 0.3% of the freestream mass-flux. This low value ensures that the noise is not too high to trigger bypass transition of the laminar boundary layer (Van Ingen, 2008). An overshoot of RMS can be observed before separation ($X^* \approx -0.35$) and is due to the Mach wave observed from the Schlieren visualisation (Figure 2). This Mach wave is considered to be quite weak as it has no significant effect on the mean flow (Figure 4) and the RMS returns to its original value after crossing this wave.

It can be seen that the shape of the curves are similar for the three Reynolds numbers, suggesting that the type of interaction is similar. A clear local overshoot of RMS can be seen around separation and reattachment, with the RMS gradually returning to its original value after both events. No exponential increase of RMS is observed after reattachment for the three Reynolds numbers.

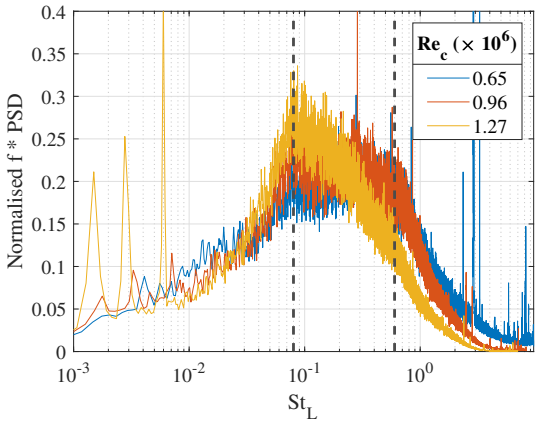

Figure 8: Pre-multiplied power spectral density at reattachment shock-wave for the three Reynolds numbers.

Looking at the spectral space for the three Reynolds numbers, Figure 8 shows the estimates of the power spectral density measured at the reattachment shock-wave in the external flow. The spectral data is represented in normalised pre-multiplied form to highlight the contribution of different frequency bands to the total energy content. Frequency is shown in the classical non-dimensional form of Strouhal number based on the length of interaction and the freestream velocity. Probe vibrations and support oscillations are magnified at the reattachment shock-wave, characterised by sharp localisation of energy at very low frequency and their harmonics ($St_L < 10^{-2}$). The shape of the spectra is similar for the three Reynolds numbers with two major time scales. A low frequency scale around $0.07 \leq St_L \leq 0.09$ and a high frequency

scale around $0.5 \leq St_L \leq 0.7$, which are more clearly visible at lower Reynolds numbers.

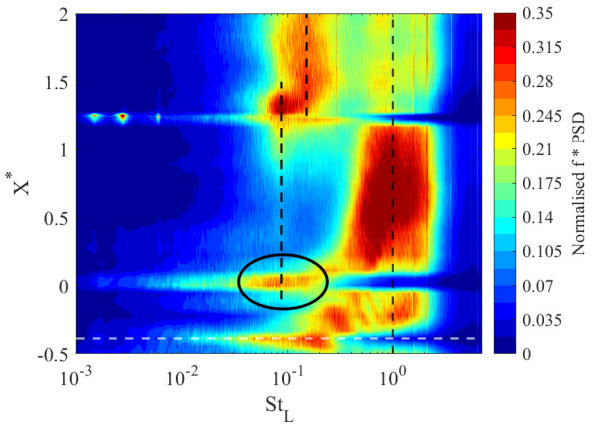

Figure 9: Longitudinal evolution of normalised pre-multiplied power spectral density at $Re_c = 1.27 \times 10^6$ for the compression ramp.

To understand the evolution of dominant frequency scales over the interaction, Figure 9 shows the contours of the normalised pre-multiplied power spectral density for the highest Reynolds number. The Mach wave observed in Figure 7 is highlighted by the dashed white line. Probe vibrations and their harmonics observed in Figure 8 can be identified here through sharp red spots at very low frequencies at the reattachment shock-wave. The overall organisation is similar for the three Reynolds numbers and hence the results for only one case is shown here.

It can be seen that most of the energy is concentrated at high frequencies before separation (notwithstanding the Mach wave). Separation of the boundary layer is associated with the same low frequency observed in Figure 8 ($0.07 \leq St_L \leq 0.09$, annotated by the black circle). On the contrary, the region over the separation bubble is associated with high frequency scales centred around $St_L \approx 1$. Low frequencies are again found at the reattachment shock-wave of the boundary layer. However, further downstream, intermediate frequency scales around $0.1 \leq St_L \leq 0.2$ are most dominant. The high frequency scales observed over the separation bubble are also found after reattachment, although not the dominant scales.

Figure 10 is a similar visualisation of the power spectral density from the hot-wire measurements of Diop (2017) for the interaction between an oblique shock-wave and a laminar boundary layer. These experiments were performed at the same Mach number for a effective flow deflection of 3.7° and Reynolds number of 0.65 million. The very low frequency content ($St_L < 10^{-2}$) around separation ($X^* = 0$) corresponds to an artefact of the experiment, possibly due to probe vibrations and support oscillations.

Comparison with Figure 9 shows that similar frequencies are involved at separation and over the mixing layer, with $St_L \approx 0.09$ (annotated by the black circle at the bottom left) and $St_L \approx 1.5$ respectively. The major difference is the concentration of most of the energy at high frequencies after reattachment (annotated by the black circle at the top right). This is associated with breakdown of coherent structures in the boundary layer leading to transition to full turbulence (Diop *et al.*, 2019).

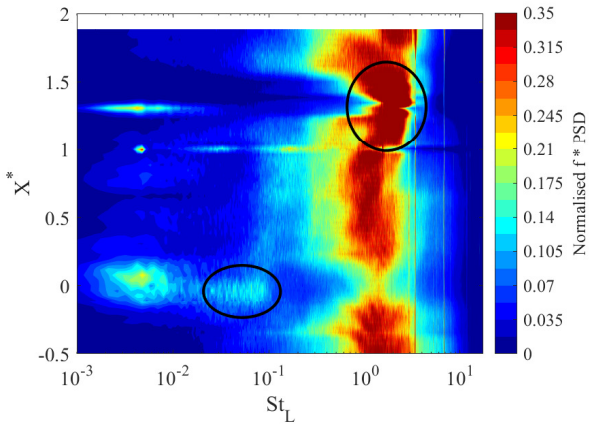

Figure 10: Longitudinal evolution of normalised pre-multiplied power spectral density at $Re_c = 0.65 \times 10^6$ from oblique SBLI (Diop, 2017).

DISCUSSION

The experiments of the oblique SBLI from Diop (2017) showed that transitional mechanisms were strongly amplified over the interaction, evidenced by exponential amplification of characteristic frequency scales associated with the mixing layer. Particularly, intermediate frequency scales ($St_L \approx 0.5$) were significantly amplified over the separation bubble. These scales were typically associated with the non-linear phase of the transition process (Mayer *et al.*, 2011). This led to transition of the laminar boundary layer at reattachment, featured by the concentration of energy at high frequencies near this region. On the contrary, there is no clear evidence of transition at reattachment in the current experiments of the compression ramp (Figures 7 and 9), even though the freestream conditions and the equivalent shock strength is the same. Correspondingly, the intermediate scales, thought to be essential for transition, are found after reattachment. Therefore, it seems that the transition to turbulence occurs at some point far downstream of reattachment. Of course, the boundary layer after reattachment is definitely altered and might not follow the shape of a canonical Blasius profile, but it is not fully turbulent either. This suggests that the compression ramp has a "fully laminar" interaction as opposed to a "transitional" type for the oblique SBLI.

This fundamental difference in the type of interaction has subtle effects on the length and time scales between the two geometrical configurations. It is known that the length scales of the compression ramp are relatively smaller compared to oblique SBLIs, due to the geometrical constraints imposed by the ramp on the reattachment of the boundary layer, as highlighted in Figure 5 . While scaling the length scales based on the respective geometrical configurations significantly reduces the large differences (Figure 6), a non-trivial difference is still observed in the slope of the curves between the two geometrical configurations. For a fully laminar interaction, as transition occurs far downstream of reattachment, the length of interaction is thought to be governed solely from a mass balance point of view (Souverein *et al.*, 2013). For a transitional interaction, the length scale is governed by a combination of mass balance and transitional mechanisms, which tend to reduce the length of interaction when Reynolds number is increased. The presence of these transitional mechanisms can be characterised by the dominance of intermediate frequency scales, which can be found over the separation bubble in the

oblique SBLI experiments and after reattachment for the compression ramp. Perhaps, the length scales of the compression ramp might show the same behaviour at higher Reynolds numbers, where transition could occur at reattachment. But this is outside the feasibility of the current experiments and hence could not be explored.

With regard to the time scales, the low-frequency unsteadiness associated with separation are mostly similar between the two configurations, even though the type of interaction is different. This suggests that the intermediate frequency scales do not play a significant role in the mechanisms of the low-frequency unsteadiness. The other part of the picture is the amplitude of unsteadiness, as Chapman *et al.* (1958) suggested that fully laminar interactions are "steady" in nature while transitional interactions are unsteady. Further investigations are necessary to understand this effect in more detail.

These results highlight the delicate effects of transitional mechanisms on the type of interaction, and consequently affecting the associated length and time scales.

CONCLUSIONS

The effect of Reynolds number on the interaction between a laminar boundary layer and shock-waves are investigated experimentally over a compression ramp. Pitot probe, hot-wire anemometry and Schlieren visualisation are performed for three Reynolds numbers, varying by a factor of two between the extreme cases. The results suggest that the interaction is of the "fully laminar" type, with transition occurring far downstream of reattachment. This is in contrast to what was found in experiments of oblique SBLIs for the same freestream conditions and shock strength, where transition occurred at reattachment. Further comparisons with oblique shock reflection cases show reduced lengths of interaction for the compression ramp and different evolutions of the length scale with increasing Reynolds numbers. However, low-frequency unsteadiness associated with separation are mostly identical for both configurations.

This work is part of the European TEAMAero project (Towards Effective Flow Control and Mitigation of Shock Effects in Aeronautical Applications). The authors would like to acknowledge the support from the European Union's Horizon 2020 research and innovation programme under grant agreement No. EC grant 860909.

REFERENCES

Ackeret, Jakob, Feldmann, F & Rott, N 1947 Investigations of compression shocks and boundary layers in gases moving at high speed. *Tech. Rep.*.

Babinsky, Holger & Harvey, John K 2011 *Shock wave-boundary-layer interactions*, , vol. 32. Cambridge University Press.

Chapman, Dean R, Kuehn, Donald M & Larson, Howard K 1958 Investigation of separated flows in supersonic and subsonic streams with emphasis on the effect of transition.

Clemens, Noel T & Narayanaswamy, Venkateswaran 2014 Low-frequency unsteadiness of shock wave/turbulent boundary layer interactions. *Annual Review of Fluid Mechanics* **46**, 469–492.

Commission, European, for Mobility, Directorate-General, Transport, for Research, Directorate-General & Innovation 2011 *Flightpath 2050 : Europe's vision for aviation : maintaining global leadership and serving society's needs*. Publications Office.

Délery, Jean, Marvin, John G & Reshotko, Eli 1986 Shock-wave boundary layer interactions. *Tech. Rep.*. Advisory Group for Aerospace Research and Development Neuilly-Sur-Seine (France).

Diop, Moussa 2017 Transition à la turbulence en écoulements compressibles décollés. PhD thesis, thèse de doctorat dirigée par Dupont, Pierre et Piponniau, Sébastien Mécanique et physique des fluides. Mécanique énergétique Aix-Marseille 2017.

Diop, Moussa, Piponniau, Sébastien & Dupont, Pierre 2017 Transition mechanism in a shock wave boundary layer interaction. In *Tenth International Symposium on Turbulence and Shear Flow Phenomena*. Begel House Inc.

Diop, Moussa, Piponniau, Sébastien & Dupont, Pierre 2019 High resolution lda measurements in transitional oblique shock wave boundary layer interaction. *Experiments in Fluids* **60** (4), 1–15.

Diop, Moussa, Piponniau, Sébastien & Pierre, Dupont 2016 On the length and time scales of a laminar shock wave boundary layer interaction. In *54th AIAA Aerospace Sciences Meeting*, p. 0073.

Doerffer, Piotr, Hirsch, Charles, Dussauge, Jean-Paul, Babinsky, Holger & Barakos, George N 2010 *Unsteady effects of shock wave induced separation*, , vol. 114. Springer Science & Business Media.

Dolling, David S 2001 Fifty years of shock-wave/boundary-layer interaction research: what next? *AIAA journal* **39** (8), 1517–1531.

Dupont, Pierre 1990 Etude expérimentale des champs turbulents dans une couche limite supersonique fortement chauffée. PhD thesis, Aix-Marseille 2.

Dupont, P, Haddad, C & Debieve, JF 2006 Space and time organization in a shock-induced separated boundary layer. *Journal of fluid Mechanics* **559**, 255–277.

Erengil, Mehmet E & Dolling, David S 1991 Unsteady wave structure near separation in a mach 5 compression rampinteraction. *AIAA journal* **29** (5), 728–735.

Mayer, Christian SJ, Von Terzi, Dominic A & Fasel, Hermann F 2011 Direct numerical simulation of complete transition to turbulence via oblique breakdown at mach 3. *Journal of Fluid Mechanics* **674**, 5–42.

Morkovin, Mark V 1956 *Fluctuations and hot-wire anemometry in compressible flows*. North Atlantic Treaty Organization advisory Group for aeronautical research ....

Piponniau, Sébastien, Dussauge, Jean-Paul, Debieve, Jean-François & Dupont, Pierre 2009 A simple model for low-frequency unsteadiness in shock-induced separation. *Journal of Fluid Mechanics* **629**, 87–108.

Smits, Alexander J & Dussauge, Jean-Paul 2006 *Turbulent shear layers in supersonic flow*. Springer Science & Business Media.

Souverein, LJ, Bakker, PG & Dupont, P 2013 A scaling analysis for turbulent shock-wave/boundary-layer interactions. *Journal of Fluid Mechanics* **714**, 505–535.

Touber, Emile & Sandham, Neil D 2009 Large-eddy simulation of low-frequency unsteadiness in a turbulent shock-induced separation bubble. *Theoretical and Computational Fluid Dynamics* **23** (2), 79–107.

Van Ingen, J 2008 The en method for transition prediction. historical review of work at tu delft. In *38th Fluid Dynamics Conference and Exhibit*, p. 3830.